Molecular Dynamics Simulations of Energy Dissipation on Amorphous Solid Water: Testing the Validity of Equipartition

Adrien Fredon, Gerrit C. Groenenboom, and Herma M. Cuppen*

Read Online

ACCESS | Metrics & More | Article Recommendations | Supporting Information

ABSTRACT: Many different molecular species have been observed in the interstellar medium. These range from simple diatomic species to saturated organic molecules with several carbon atoms. The latter molecules are assumed to be formed predominantely on the surface of interstellar dust grains. All surface reactions that can proceed under the low interstellar temperatures are exothermic. Their exothermicity can be as high as a few electron volts, which is considerable compared to the thermal energy of the molecules at 10 K. It is postulated that this exothermicity can be used for the desorption of reaction products from the grain. In previous studies, we have shown that translational excitation can lead to desorption, whereas vibrational and rotational excitations are much less efficient in the desorption of surface products. Vibrational excitation is however much more likely upon bond formation than translational excitation. The present study follows energy dissipation upon translational, vibrational, or rotational excitation of admolecules on a surface and its conversion, or lack thereof, to different energy contributions. To this end, thousands of molecular dynamics simulations were performed with an admolecule on top of a surface that received a fixed amount of energy, vibrational, rotational, or translational. Three different surface species have been considered, CO_2, H_2O, and CH_4, spanning a range in binding energies, the number of internal degrees of freedom, and molecular weights. A fast exchange of energy between vibrational stretches is observed, but only very limited exchange to rotational or translation excitation has been found. For the dissipation of energy to the surface, excitation of the surface−admolecule bond is critical. Astrochemical models often assume instantaneous equipartition of energy after a reaction process to estimate the amount of available energy for chemical desorption. Based on the present study, we conclude that this assumption is not justified.

KEYWORDS: *interstellar ice, energy dissipation, grain surface chemistry, astrochemistry, molecular dynamics*
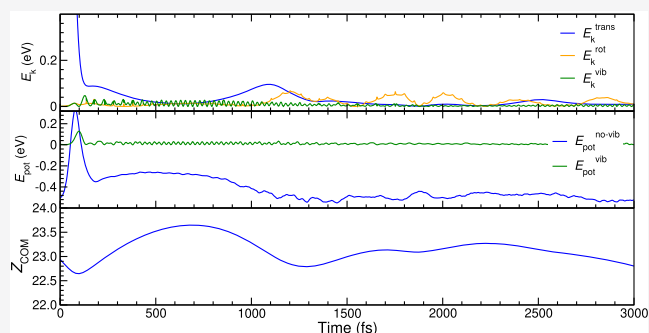
1. INTRODUCTION

Nowadays, we know that dust grains are omnipresent in the denser parts of the interstellar medium (ISM), and grain surface chemistry plays a key role in the formation of numerous chemical species even in environments of low density. Several saturated molecules, which are thought to have formed on these dust grains, are observed in the gas phase of dark molecular clouds despite their low temperatures.[1−4] Since thermal desorption of these species from the grain cannot account for their presence in the gas phase, other mechanisms have to be considered. In the present paper, we will focus on reactive or chemical desorption, where the excess reaction energy is used to facilitate desorption. The aim of this study is to understand whether and how the energy is redistributed after the formation of the chemical products. Previous work[5] involved pure translational excitation of CO_2, H_2O, and CH_4 adsorbed on the amorphous ice surface. We found that translational excitation can indeed result in diffusion and desorption. However, excess energy is likely to be also released into rotational and vibrational modes. In follow-up work, we

showed that vibrational and rotational excitons are not as effective in releasing products from the ice surface.[6] An important point in this respect is how the energy is initially partitioned. Due to the lack of any other information, often equipartition is assumed, where the energy released in reactions is equally distributed among all degrees of freedom[7] or among vibrational degrees of freedom including binding to the surface.[8] For bond-forming reactions, the formed bond is however more likely to be excited, and in dissociation reactions, rotational and translational excitations likely dominate.

A major goal of the present study is to test the validity of the equipartition assumption by studying the time scale for
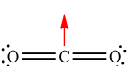
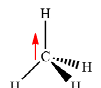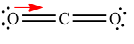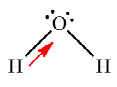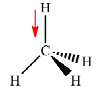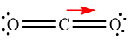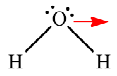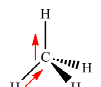**Table 1. Initial Distribution of the Vibrational Potential Energy over Bonds (B) and Angles (A) for the Different Types of Vibrational Excitations**

	CO_2	H_2O	CH_4
Type 1			
E_B^{pot} (eV)	[0.21, 0.25]	[0.60, 0.69]	[0.71, 0.75]
E_B^{pot}/n_B	$2 \times$ [0.105, 0.125]	$2 \times$ [0.30, 0.345]	$1 \times$ [0.53, 0.57] + $3 \times$ [0.06, 0.07]
E_A^{pot}	[0.75, 0.79]	[0.31, 0.40]	[0.25, 0.29]
E_A^{pot}/n_A	[0.75, 0.79]	[0.31, 0.40]	$3 \times$ [0.05, 0.06] + $3 \times$ [0.03, 0.04]
Type 2, 3			
E_B^{pot}	1	1	1
E_B^{pot}/n_B	0 and 1	0 and 1	$1 + 3 \times 0$
E_A^{pot}	0	0	0
E_A^{pot}/n_A	0	0	0
Type 4			
E_B^{pot}	1	[0.98, 0.99]	[0.74, 0.78]
E_B^{pot}/n_B	0.5	[0.44, 0.48] + [0.49, 0.54]	$1 \times$ [0.43, 0.46] + $1 \times$ [0.21, 0.23] + 2×0.05
E_A^{pot}	0	[0.01, 0.02]	[0.22, 0.26]
E_A^{pot}/n_A	0	[0.01, 0.02]	$6 \times$ [0.02, 0.07]

redistribution of internal energy over different vibrational, rotational, and translational modes. The paper is organized as follows. First, the methodology is described, Section 3 discusses the internal redistribution of vibrational energy and compares this against dissipation of this energy to the ice surface, and Section 4 studies the interconversion between translational, rotational, and vibrational excitations.

2. METHODOLOGY

2.1. Interaction Potentials. We used the same fully flexible interaction potentials as previously, and all potentials and parameters are described in detail in section "Interaction Potentials" of our previous papers.[5,9] For H_2O, we use the q-TIP4P/f potential,[10] which is a flexible version of the TIP4P/2005 potential[11] to prevent dissociation of O−H upon the introduction of the vibrational energy. The intramolecular interactions for CO_2 and CH_4 have been taken from refs 12 and 13, respectively. The intermolecular H_2O−CO_2 interaction is taken from Karssemeijer et al.[14] For H_2O, the charge model of the q-TIP4P/f potential is used. For the H_2O−CH_4 interactions, we refitted the H_2O−CH_4 PES_{2b}-CSM potential by Qu et al.[15] with a Beck potential. The dispersion contribution is cut off at 11.0 Å, and the Coulombic part of the potential is computed using a particle−particle particle−mesh solver with a relative root-mean-square error in per-atom force of 10^{-6}.

2.2. Rotational Excitations. Over a large set of simulations, a fixed amount of rotational energy is randomly distributed over the three (two for CO_2) rotation axes. This section explains how this is obtained; the derivation of this method can be found in the Supporting Information. The inertia tensor of the admolecule $\mathbf{I}$ is diagonalized to obtain the three principal axes $\mathbf{u}_i$ and the three moments of inertia I_i. The $\mathbf{u}_i$ vectors define the body fixed (BF) frame. The total rotational energy is

$$E_{rot} = \sum E_i \tag{1}$$

where E_i is the rotational energy associated with eigenvector $\mathbf{u}_i$. A random point in spherical coordinates with radius 1 is generated through

$$\phi = \frac{\pi}{2}\text{rand}[0, 1] \tag{2}$$

and

$$\theta = \arccos(\text{rand}[0, 1]) \tag{3}$$

The corresponding $\mathbf{r}$ vector in the BF frame can then be applied to obtain E_i, where i runs over the three dimensions of $\mathbf{r}$

$$E_i = r_i^2 E_{rot} \tag{4}$$

and the angular velocity vector $\boldsymbol{\omega}^{BF}$

$$\omega_i^{BF} = \pm\sqrt{\frac{2E_i}{I_i}} \tag{5}$$

The $\pm$ sign is chosen randomly. By applying $\mathbf{U} = [\mathbf{u}_x, \mathbf{u}_y, \mathbf{u}_z]$, we can return to Cartesian coordinates

$$\boldsymbol{\omega}^{CF} = \mathbf{U}\boldsymbol{\omega}^{BF} \tag{6}$$

and obtain the velocity associated to the rotation for each atom A using

$$\mathbf{v}_A = \boldsymbol{\omega}^{CF} \times \mathbf{r}_A^{com} \tag{7}$$

where $\mathbf{r}_A^{com}$ is the position vector of atom A relative to the center of mass.

For the analysis of the results, the reverse procedure is used to separate the different kinetic energy contributions. First, the center-of-mass velocity of the molecule is obtained and subtracted for the translational energy, and next, the rotational

energy is obtained by the reverse process described above. The remaining kinetic energy is assumed to be due to vibration.

2.3. Vibrational Excitations. The vibrational excitations are realized by a conformational change in the geometry of the admolecule. We used four different methods, which are schematically depicted in Table 1. In method 1, the central atom (C for CO_2, O for H_2O, and C for CH_4) is displaced from its original position to both stretch and bend the different internal modes of the admolecule. For CO_2, the carbon atom is displaced perpendicularly with respect to the O−O axis, thus elongating the two CO bonds and bending the OCO angle. For H_2O, the oxygen atom moved along the bisection of the HOH angle, compressing the two HO bonds and bending the HOH angle. In the case of CH_4, the carbon atom is displaced along one of the CH bonds, thus compressing this latter bond and elongating the three others bonds.

For the second and third methods, only one specific bond is excited instead of a combination of bonds and angles by moving one of the terminal atoms (O for CO_2, H for H_2O, and H for CH_4) with respect to the central atom to affect only one bond. Considering that the admolecule is surrounded by H_2O surface molecules, compression of the bond is preferred over elongation to avoid atoms approaching the surface at too close distance. For both methods, one bond is contracted by moving one H atom for H_2O and CH_4 or one O atom for CO_2. For method 2, the atom pointing away from the surface is chosen, and for method 3, the atom pointing toward the surface is chosen.

For the fourth and last method, nonsymmetric and antisymmetric excitations are performed. For CO_2, the carbon atom is moved toward one of the oxygen atoms, thus compressing one bond and elongating the other. For H_2O, the oxygen atom is displaced parallel to the H−H axis, thus elongating the one bond and shortening the other and bending the HOH angle. In the case of CH_4, the carbon atom is moved toward one of the hydrogens, while another nonhydrogen bonded hydrogen is moved toward the carbon atom, thus compressing two bonds and bending all of the angles.

The vibrational energy as a function of the displacement of the moving atom (see Table 1) is calculated for isolated molecules with a step size of 0.01 Å and then interpolated using a third-order polynomial. Since there is a direct, one-to-one mapping of the displacement to one energy value and *vice versa*, only one displacement can be used for each vibrational energy value per admolecule and per binding site on the surface. For this reason, the number of different vibrational excitation realizations is limited to ten, instead of the thousands that can be achieved for translational and rotational excitations. Only if translational excitation is used in combination with other excitation types, large statistics can be obtained. One should realize this for the interpretation of the results later on. The vibrational excitations induce a structural change in the admolecule, which modifies its inertia tensor. Hence, we apply the rotational excitation after displacing the atoms.

Table 1 further indicates the different ways in which the vibrational potential energy is initially distributed among the different vibrational modes (bonds and angles) for each type of vibrational excitation. In this table, E_b^{pot} and E_a^{pot} stand for "bond potential energy" and "angle potential energy", respectively, while E_b^{pot}/n_b and E_a^{pot}/n_a stand for "bond potential energy per bond" and "angle potential energy per angle", respectively. For some specific modes, the potential energy in

this mode depends on its initial configuration in a specific binding site and a range is given. The bold numbers indicate how many bonds/angles belong to a specific range/value of energy.

2.4. Simulation Procedure. Molecular dynamics simulations were performed for each of the three different admolecules on top of an ASW surface. After equilibration, the admolecule was given an additional amount of translational, rotational, and/or vibrational energy. Energy transfer in this out-of-equilibrium system was then followed. To obtain statistics on this process, thousands of independent simulations were performed. The equations of motion are integrated over time using the standard velocity-Verlet integrator. All simulations are performed using the LAMMPS package (version 16/02/16).[16] An amorphous sample of 360 H_2O molecules is used. The production of the ice is detailed in our previous paper.[5] In brief, the sample is prepared by hyperquenching a liquid water sample in a periodic, cubic box with lengths of roughly 22 Å. To create a slab model, the z-axis is increased by 100 Å, after which the sample is further relaxed at 10 K.

To trace the variations in binding sites, 1000 NVT equilibration simulations are performed for each of the three admolecules. For each run, the initial position of the molecule is randomly chosen in x and y directions and $\Delta z = 7$ Å above the surface. The orientation of the admolecule with respect to the surface is also chosen randomly. To promote binding to the surface, the molecule is given a low initial velocity towards the surface. A Nosé−Hoover thermostat was used at a temperature of 10 K. In each of the energy dissipation simulations, the admolecule is excited at the start of the simulation in such a way that we can select the type of mode in which the energy is stored.

Many sets of simulations have been performed to span the different combinations of excitations. All of these simulations are performed within the NVE ensemble to ensure that no energy was artificially taken from the system. Table 2 summarizes them. Throughout the paper, we will refer to these series of simulations by their label. For each series, the minimum and maximum values of the excitation energy are indicated. The increment is 0.5 eV for all series. Vibrational

Table 2. Sets of Molecular Dynamics Simulations Indicating the Amount of Translational, Rotational, and Vibrational Energy Given to the System[a]

series	E_{trans} (eV)	E_{rot} (eV)	E_{vib} (eV)	no. of trajectories per energy value	vib type
A	1	0	1	5000	1
B	1	0	1	5000	2
C	1	0	1	5000	3
D	1	0	1	5000	4
E	0	0	0.5−5	10	1
F	0	0	0.5−5	10	2
G	0	0	0.5−5	10	3
H	0	0	0.5−5	10	4
I	0.5−5	0	0	2000	-
J	0−4	0	1	2000	1
K	0−4	1	0	2000	-

[a]Hyphen indicates the range of energies within one series. The type of vibrational energy (see Table 1) is indicated in the case of vibrational excitation. The number of trajectories per energy combination is given for each series.

excitation is initially given by additional potential energy, whereas rotational and translational excitations are achieved by adding kinetic energy. Different trajectories for each energy combination are obtained using different starting positions (ten in total) and different initializations of the kinetic energy, if applicable.

3. INTERNAL RELAXATION VS ENERGY DISSIPATION OF VIBRATIONAL ENERGY

This section discusses the dissipation of vibrational energy, where the vibrational energy can be injected in different ways as it is done in simulation series A through H. Vibrational excitation of an admolecule can be dissipated through different channels: the admolecule can release this energy to the surface (channel vs), the energy can be converted into translational (vt) or rotational energy (vr), and the vibrational energy can be redistributed among other vibrational degrees of freedom (channel vv). These dissipation processes are not instantaneous, and their relative rates will determine the competition between these channels and the long time scale dynamics of the system. The resulting deformation or restructuring is likely different when an admolecule releases all of its energy into the ice in either 1 fs or 1 ps. This concept also applies to internal relaxation where energy might be trapped in a specific vibrational mode for a long time or be redistributed among all modes very quickly, offering new energy dissipation channels.
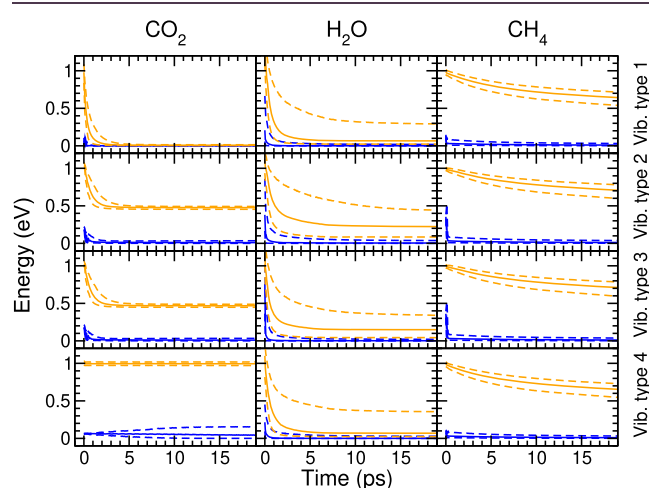
Figure 1. Time evolution of the total vibrational energy E_{vib}^{tot} (orange lines) and C_{vv}^*, a measure of the internal vibrational reorganization time scale (blue lines). Each panel shows the median value for 5000 simulations (solid curves) as well as the 10 and 90 percentiles (dashed curves).

Figure 1 shows the time evolution of the total vibrational energy E_{vib}^{tot} and C_{vv}^*. The variable C_{vv}^* is used to quantify the vv channel and is the variance of the vibrational potential energy

$$C_{vv}^* = \sum_{i}^{\nu_{vib}} \left(E^{pot,i} - \frac{E^{pot,tot}}{\nu_{vib}} \right)^2 \tag{8}$$

where the sum runs over all bonds and angles in the molecule. Their total number ν_{vib} is 3, 3, and 10 for CO_2, H_2O, and CH_4, respectively. E_{vib}^{tot} is the sum of potential and kinetic vibrational

energy. Both E_{vib}^{tot} and C_{vv}^* are computed at each timestep and are plotted here for four different types of translational–vibrational excitations (series A, B, C, and D in rows) and for the three admolecules in columns. In these series, the translational and vibrational energies are both 1 eV and the translational excitations always point downward to promote energy transfer between the admolecule and the surface. Each panel shows the median energy, E_{vib}^{tot}, in black, and C_{vv}^*, in blue, for 5000 simulations as well as the 10 and 90 percentiles, so there are six lines in each panel.

The graphs in Figure 1 are very different for the three admolecules. For CH_4, the internal relaxation C_{vv}^* occurs very quickly (within 1 ps), while dissipation to the surface is slow. This is visible from E_{vib}^{tot}, which still decreases after 20 ps. This is independent of the excitation type chosen. For CO_2, we observe a strong disparity between the results for different types of vibrational excitations. The most remarkable result is observed for type 4, which is the asymmetric stretch of CO_2: the initial vibrational energy remains in the admolecule throughout the entire simulation. The central carbon atom vibrates, alternately exciting the two CO bonds, while the two oxygen atoms remain more or less stationary. It clearly shows that to transfer vibrational energy from the admolecule to the surface, the surface–admolecule bond should be excited first, which is not the case for this particular excitation method. For H_2O, we observe an intermediate trend between CO_2 and methane: initially, C_{vv}^* is much faster than the loss of vibrational energy, but not all energy is transferred to the surface. The internal relaxation occurs within 2 ps for all excitation types, whereas the loss of internal energy occurs in 6−8 ps for vibrational excitation types 1, 3, and 4 or 10−12 ps for vibrational excitation type 2. The vibrational excitation types 2 and 3 both involve the stretch of one of the two OH bonds of the admolecule. The difference in energy loss rate between these two types can be explained by the fact that for type 2 the hydrogen involved in the excitation is not participating in the hydrogen bond network of the surface, whereas it is participating for type 3. Again, first the surface–admolecule bond needs to be excited before dissipation can occur. For type 2, the initial vibrational energy first needs to be transferred internally to the other bond, which increases the dissipation time scale for type 2 with respect to type 3 excitation. Additionally, the asymptotic limit for E_{vib}^{tot} depends on the excitation type. For types 2 and 3, the final E_{vib}^{tot} is around 0.2− 0.25 eV, while it is 0.1 eV for types 1 and 4. The trajectories of type 4 for H_2O show that moving the oxygen along the H−H axis leads to a quick equilibration of the two hydrogens with respect to the new oxygen position. During this equilibration, the hydrogens move quickly with respect to the surface. The same observation is made for type 1 but not for types 2 and 3, which explains why less energy is dissipated to the surface for types 2 and 3, similarly to what was observed for CO_2.

These results clearly show that the vibrational modes are not equivalent and that the type of vibrational excitation can have a strong effect on the importance of the energy dissipation channels (C_{vt}^*, C_{vr}^*, C_{vs}^*). In general, we can conclude that internal relaxation between bonds is fast but that it only leads to surface dissipation if the initial excitation also excites the surface–admolecule bond. For CO_2, angular vibration is required for this to occur and bond-to-angle relaxation does not appear to occur so efficiently. We did not observe any sign of C_{vt}^* and C_{vr}^* channels, meaning that most of the initial energy present in the admolecule is dissipated into the ice.

The curves in Figure 1 are averaged over many simulations. At the individual bond and simulation level, $E^{pot,i}$ is much less smooth and not straightforward to interpret. Bond energies fluctuate strongly in time and are constantly redistributed among the different bonds. Depending on the vibration type, not all angular modes become excited. The spread of vibrational energy goes quickly.

Pantaleone et al.[17] have used *ab initio* MD to study the relaxation of the HCO radical in detail. They show that 90% of the reaction energy dissipates to the water ice in 1 ps. The dissipation process starts with the increased vibration of one of the surface–reactant bonds after which the hydrogen-bonding network of the crystalline substrate quickly distributes the energy over the ice. The importance of the surface–admolecule bond is further suggested by the rate of dissipation of CH_4, which is much slower than for the other two molecules. The interaction between CH_4 molecules is also much weaker. However, the difference in the number of internal degrees of freedom can also play a role here. This is nine for CH_4 and only three and four for H_2O and CO_2, respectively. This means that the average energy per mode is much smaller. Likely, both effects play a role here.

Figure 2 shows the time evolution of the nonbonded energy within the substrate for CO_2 excitation of two different
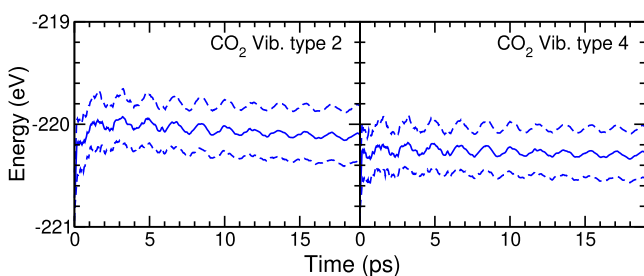
Figure 2. Time evolution of the nonbonded interaction for the substrate molecules. Each panel shows the median value for 5000 simulations (solid curves) as well as the 10 and 90 percentiles (dashed curves).

vibration types. Again, the median values averaged over 5000 trajectories and the 10 and 90 percentiles are shown. For vibration type 4, no vibrational de-excitation was found, and hence, this could be seen as a baseline. For vibration type 2, 0.5 eV of energy was lost to the surface. The vibrational energy dissipation occurs in 2 ps, and indeed, in this time frame, an additional increase in the nonbonded energy for vibration type 2 can be observed. This increase is roughly 0.25 eV w.r.t. vibration type 4. This accounts for half the dissipation energy. We found a similar increase in the translational kinetic energy of the substrate (not shown). For both sets, oscillations around an intermediate value can be observed. This indicates some kind of vibration inside the substrate. At a long time scale, this intermediate value decreases. Fitting both median curves to a cosine with a linearly decreasing baseline shows that the reduction in nonbonding energy is roughly twice as large for vibration type 2 as for vibration type 4. At the same time, an increase in the kinetic energy of the substrate for vibration type 2 can be observed. This suggests that the vibrational energy of the admolecule is used to stabilize the substrate.

The results presented in Figure 1 are based on series A, B, C, and D, which have both vibrational and translational excitations. Series E, F, G, and H, which consist of pure

vibrational excitations of types 1, 2, 3, and 4, respectively, give very similar results, and hence, the C^*_{vv} channel appears independent of the addition of translational energy.

4. ENERGY INTERCONVERSION

The previous section showed that vibrational energy quickly distributes over the different vibrational energy modes. The assumption of instantaneous equipartition hence appears justified for vibrational energy. The present section studies the interconversion of translation energy to rotational and vibrational energy and *vice versa*. Hence, simulations will be presented also with rotational and translational excitations and a combination thereof is discussed.

Figure 3 shows the time evolution of different kinetic energy components (E_k^{trans}, E_k^{rot}, E_k^{vib}) and potential energy components
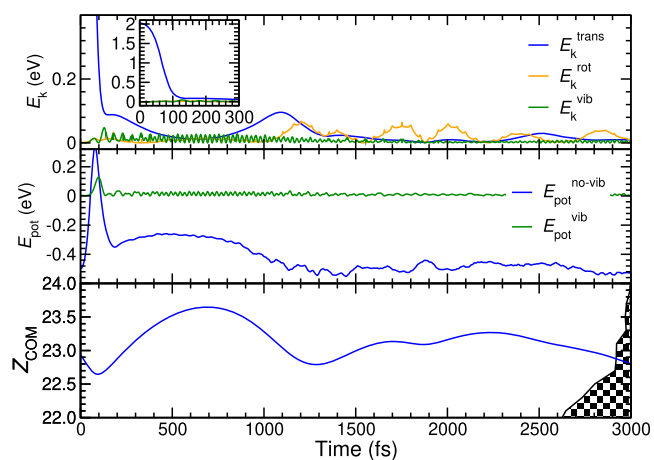
Figure 3. Time evolution of different energy components of a CO_2 admolecule during a simulation in which this latter was excited with 2 eV of translational energy. The top panel shows all of the components linked to the kinetic energy (translational, rotational, vibrational, and total kinetic energy), the middle panel shows the absolute value of all the components linked to the potential energy (bonded, nonbonded, and total potential energy), and the lower panel shows the height of the center of mass of the admolecule. The ice surface is located at around 22.5 Å, as indicated by the number density profile in black.

(E_p^{tot}, $E_p^{nonbond}$, E_p^{vib}) of a CO_2 admolecule that is translationally excited. This simulation is part of series I. The inset in the top panel shows the same kinetic energy information but with different dynamic ranges. The bottom panel shows the *z*-coordinate of the center of mass of the molecule, with the surface located at around 22.5 Å. It shows that the admolecule hits the surface after roughly 50 fs and then bounces over the surface a few more times. A rapid change in the kinetic energy can be seen at most of these bounces; the most dominant change is at the first bounce. This can best be seen in the inset. At this first bounce, most of the initial translational energy is rapidly lost. This coincides with an increase in vibrational energy, which accounts for roughly 2% of the kinetic energy loss. The vibrational time scale for CO_2 in the gas phase is 13 fs, For the excited CO_2, it is roughly twice as long, 25 fs, as estimated from Figure 3. The vibrational energy is quickly lost to the surface. This again hints at the role of surface–admolecule vibrational excitation. Later interactions with the surface result in some rotational movement. The CO_2 slowly finds more and more stable binding sites, resulting in a decrease, or more negative, of the potential energy.
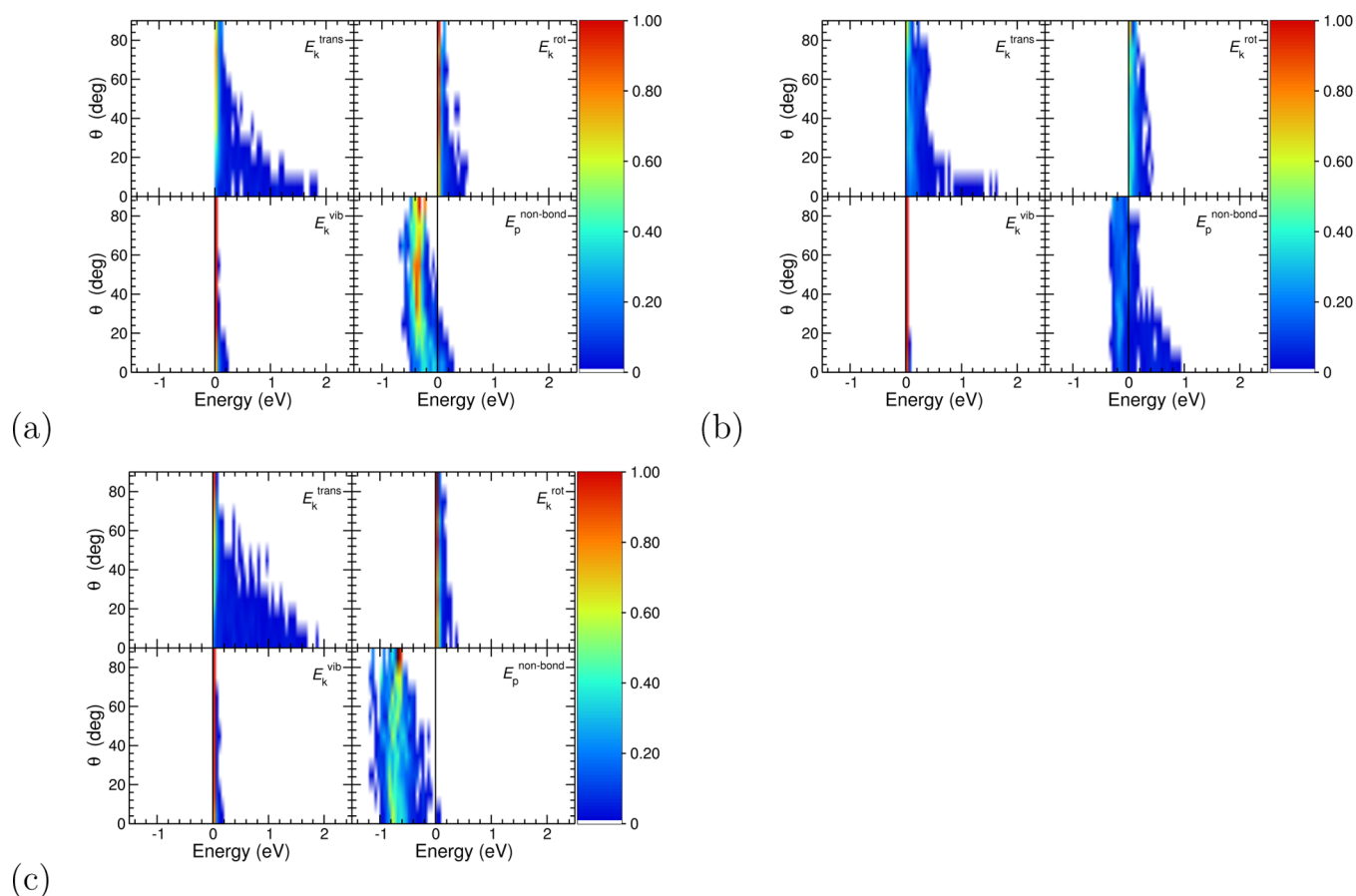
Figure 4. Distribution of the energy stored in an admolecule after a bounce on the surface for a translational excitation of 2 eV. Each panel is divided in for subplots, each of them showing a different component of the energy (E_k^{trans}, the kinetic energy stored in translation; E_k^{rot}, the kinetic energy stored in rotation; E_t^{vib}, the total energy stored in vibration; and $E_p^{nonbond}$, the potential interaction energy between the admolecule and the surface). Angle θ represents the incident angle with which the admolecule bounces on the surface ($\theta = 90$ represents normal incidence). The color legend represents the normalized number of counts; the normalization is set to 1 for each subplot and each angle θ. All of the squares with values below 1% are set to appear white. The vertical black lines show the 0 eV bin. Panel (a) is for CO_2, (b) for CH_4, and (c) for H_2O.

4.1. Translational Energy Interconversion.

Figure 3a shows the results for only one simulation; one starting binding site, one type of excitation, one incident angle, and one admolecule. To understand the general trends in energy transfer, we have summarized our results over many simulations in Figure 4−6. In all of these simulations, the admolecule received translational energy, sometimes in combination with vibrational or rotational energy. We focus specifically on those trajectories where the admolecule bounces on the surface since we expect energy transfer to be most effective at such a scattering event, as seen in Figure 3. Figure 4a shows a series of 2D histograms representing energy distribution over the different components of a CO_2 admolecule just after the first scattering with the surface. The y-axis represents the incident angle with respect to the surface of the initial momentum given to the molecule, the x-axis represents the energy in each component after the bounce, and the color indicates the relative occurrence of such a combination. These histograms take into account hundreds of independent simulations in which the admolecule is initially given 2 eV of pure translational energy in a random direction. These simulations belong to series I. The inelastic collisions are very complex, and the energy transfer takes some time to occur. From simulation to simulation, this energy-transfer time varies between 2−3 and 7−8 fs. To ensure that the admolecule

has time to dissipate its energy during the bounce, we register the energy components 10 fs after the velocity of the center of mass of the admolecule has a positive z-component.

The top-left subplot shows the amount of translational energy that remains in the admolecule after the bounce. For a small θ angle—when the approach is near parallel to the surface—, up to 1.7 eV of the initial energy can remain in CO_2 after the bounce. The remaining translational energy decreases with increasing angle because the energy transfer is much more efficient for head-on collisions. This trend is observed for all three admolecules, as can be seen by comparing the three panels in Figure 4, although it is less clear for CH_4. Examination of the corresponding trajectories shows that CH_4 rolls over the surface at low incident angles, whereas CO_2 and H_2O do not. Indeed, a slight increase in rotational energy of 0.05−0.1 eV can be observed (top-right subplot). An energy transfer of more than 0.05 eV from translational to rotational excitation occurs in 32, 27, and 59% of the simulations for CO_2, H_2O, and CH_4, respectively. This is in agreement with the observed rolling movement of the isotropically shaped CH_4 molecules. The frictional force that is caused by this rolling movement increases the energy lost by the admolecule to the surface compared to CO_2 and H_2O. At high impact angles, the energy transfer is less efficient for CH_4 compared to CO_2 and H_2O due to its weaker interaction with the surface.
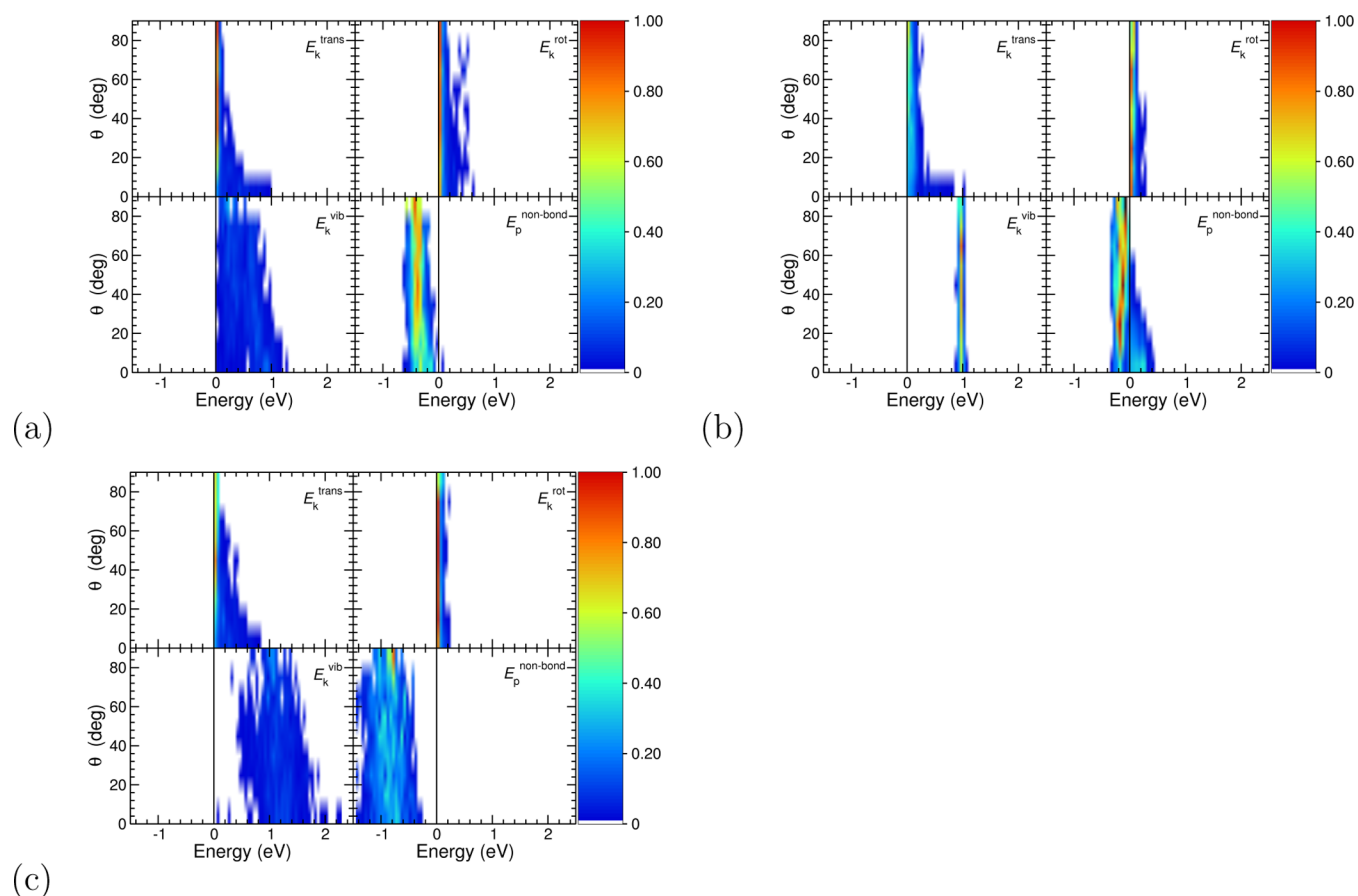
Figure 5. Distribution of energy in an admolecule 10 fs after a bounce on the surface for excitation with 1 eV of translation and 1 eV of vibration. For a detailed explanation of the panels, see Figure 4. Panel (a) is for CO_2, (b) for CH_4, and (c) for H_2O.

The bottom-left subplot shows the vibrational energy in the admolecule after the bounce. For the three admolecules, only a small amount, 0.2 eV at most for H_2O, is transferred from translational to vibrational energy. Contrary to our initial expectations, this conversion is less efficient at normal incidence than at the glancing angle. We think this is because at a glancing angle the interaction time with the surface is much longer, and since the coupling of translational and vibrational energy proceeds via the surface−admolecule bond, there is more opportunity for this transfer to occur.

Finally, the nonbonded interaction energy between the admolecule and the surface is presented in the bottom-right panel. This is the only energy contribution that can have both positive and negative values. In principle, positive values should be repulsive and lead to desorption, but one should realize that we record this contribution only 10 fs after the bounce and the molecule might need more time to relax to the most optimal binding configuration or is still moving. Indeed, it can be observed that the binding energy decreases, or becomes more negative, with the incident angle for all three admolecules. This appears to be anticorrelated with the amount of translational energy left in the admolecule.

Molecules approaching under glancing angles have not come to a full stand still after the first bounce and have hence not relaxed to a strong binding site.

4.2. Vibrational Energy Conversion. Figure 5 shows similar 2D histograms where the admolecules received an excitation of 1 eV of translational energy and 1 eV of

vibrational energy (series J). The total excitation energy is hence the same as in the previous graphs.

Figure 5a can be directly compared to Figure 4a, which shows the results for pure translational excitation. The top-right subplot is the same for both cases, indicating that there was conversion of vibrational energy to rotational energy. The top-left translational energy plot is again very similar in both panels when considering that the translational excitation is only 1 eV in Figure 5a. From this, we can conclude that translational energy dissipation is rather independent of the vibrational energy of the molecule. As reported in ref 6, vibrational excitation also has no influence on chemical desorption probability, which depends solely on the amount of translational energy available. However, the two bottom subplots in Figures 4a and 5a are different. We can clearly see that a large part of the initial vibrational excitation is still present. There appears to be a slight dependence on the incoming angle, where head-on collisions are more efficient in dissipating energy, similarly to the dissipation of translational energy. The nonbonded interaction energy between the admolecule and the surface in the bottom-right subplot is also clearly different. Only negative, attractive interactions are found. This cannot be fully explained by the lower initial translational energy since still several trajectories can be found with some translational energy left after the bounce. We believe that some of the vibrational energy is dissipated to the surface−admolecule bond, aiding in the relaxation of the molecule in a good binding position. There is however a time component. The
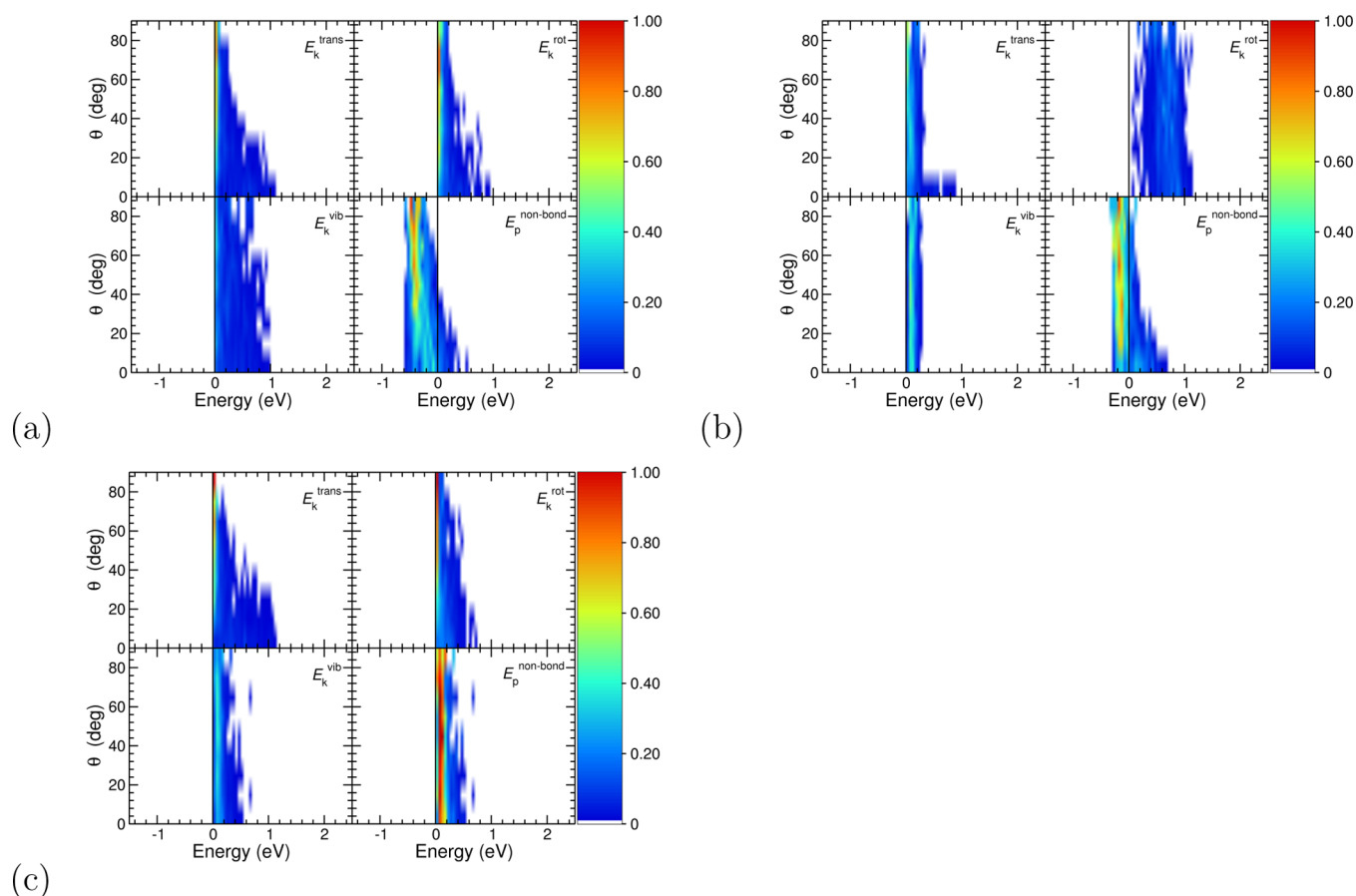
Figure 6. Distribution of the energy stored in a CO_2 admolecule after a bounce on the surface for excitation with 1 eV of translation and 1 eV of rotation. Panel (a) is for CO_2, (b) for CH_4, and (c) for H_2O.

admolecule−surface bond will first be excited—$E_p^{nonbond}$ is higher in energy—before relaxation can occur.

Figure 5b for CH_4 is very different. Here, we see from the bottom-left subplot that the vibrational energy is not dissipated immediately following the scattering event. This is indeed in agreement with Figure 1, which shows that even after 20 ps an appreciable amount of energy is still present in the admolecule, although internal vibrational relaxation is fast. The remaining three subplots in Figure 5b mimic those in Figure 4, taking into account the lower translational excitation energy. The bottom-right subplot still shows the dependence on the incoming angle, which was missing in Figure 5a for CO_2. This is another indication that the vibrational dissipation for CO_2 has aided the relaxation of the molecule in a surface site.

In general, one can conclude that vibrational energy dissipates to the ice mantle through excitation of the surface−admolecule bond. There is very little conversion to rotational or translational energy. Especially, the latter contribution is important for reactive desorption.

4.3. Rotational Energy Conversion. Finally, Figure 6 shows similar plots for simulations with 1 eV of translational excitation and 1 eV of rotational excitation. These simulations belong to series K. Again these can be compared to the simulations with pure translational excitation. Since the plots describe the dissipation immediately after a scattering event, translational excitation is required to initiate this bounce, and hence, it is not possible to make a similar plot with either pure rotational or pure vibrational excitation. Again, the additional rotational excitation does not appear to interfere with the

translational energy dissipation. For CO_2, however, a clear conversion from rotational to vibrational energy can be observed. The 1 eV rotational excitation is clearly reduced, whereas in the bottom-left panel, vibrational excitation can be observed. For CH_4, a similar effect can be observed, although much weaker. Simulations of individual H_2O, CH_4, and CO_2 molecules also show conversion from rotational to vibrational energy. This is shown in Figure 7 by the solid curves. Here, the average vibrational energy of the admolecule 15−20 ps after the initial excitation is plotted. The curves are the results of 2000 simulations. For both the solid and dashed curves, 1 eV of rotational energy is given to the molecule. The difference is that the admolecule is on top of an ASW for the dashed curves and is isolated for the solid curves. For the dash-dotted curves, the admolecules are on the surface and experience 1 eV of translational and 1 eV of rotational excitation. The dash-dotted and solid lines are very similar. This means that the conversion between rotational energies is not due to the surface but is inherent due to the centrifugal pull on the bonds during the rotation. For isolated CH_4 (the solid green curve), the conversion is always roughly the same since the effect does not depend strongly on the rotational axis due to its tetrahedral shape. The solid blue curve clearly shows that this is quite different for CO_2, where the exact amount of vibrational conversion depends strongly on the rotational axis. Again, H_2O is somewhere in between. When admolecules are adsorbed on a surface, the vibrational excitation quickly dissipates through the surface−admolecule bond as can be seen by the dashed curves that peak in the lowest bin. When the admolecule also
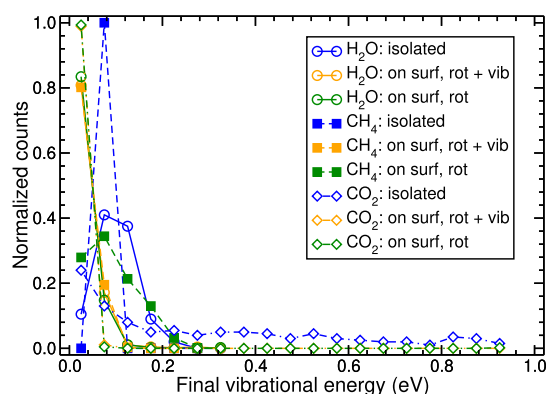
Figure 7. Long-time vibrational energy in the admolecule after 1 eV of rotational excitation. The solid lines represent simulations of isolated molecules. The dashed lines represent simulations where the admolecule is on the surface. The dash-dotted lines represent simulations in which the admolecule is on the surface and has received an additional excitation of 1 eV of translational energy. The values of the vibrational energy are averaged between 15 and 20 ps after the initial excitation.

experiences translational motion, there is no "stationary" admolecule–surface bond that can help dissipate this energy and the final vibrational energy is only slightly reduced compared to the isolated molecule.

5. DISCUSSIONS AND CONCLUSIONS

In conclusion, our results show that dissipation of vibrational energy goes through the surface–admolecule bond to the ice surface as vibrations and hence heats the ice. The rate at which this dissipation process occurs depends on whether the surface–admolecule is excited, the interaction strength, and the internal degrees of freedom of the admolecule. Weaker interaction and more degrees of freedom will lead to slower dissipation. Some of this energy is applied for stabilization or annealing of the ice structure.

Interconversion of different types of energy hardly occurs. Some rotational energy can, however, be converted into vibrational energy. The coupling between translational and ro-vibrational energy is minimal. In previous studies, we showed that it is the translational excitation that can lead to reactive desorption or nonthermal diffusion. Both processes are important for the understanding of interstellar surface chemistry. Reactive desorption is required to explain how complex molecules that are likely formed on dust grains are detected in the gas phase of cold dark regions. Nonthermal diffusion allows reaction products to move some distance over the surface before they thermalize, with the possibility to meet reactive species on the way. However, these processes will occur only if at least part of the excess energy is available in the translational form. For bond-forming reactions, most of the excess energy likely goes to the excitation of the formed bond, while in dissociation reactions, rotational and translational excitations likely dominate.

Another possibility for desorption is by electronic excitation, which was not treated in this work. Indeed, van Hemert et al.[18] showed that electronic excitation of CO can lead to desorption. Here, the admolecule–surface interaction changes upon electronic excitation, making the interaction repulsive. Vibrational excitation of CO was found to be inefficient for desorption, in agreement with our work.

Finally, let us return to the assumption of equipartition that is generally used in astrochemistry. The present work shows that this assumption is justified only for the vibrational excitation within the molecule since this spreads rather easily. Between different types—vibration, rotation, and translation—, this is not justified.

■ ASSOCIATED CONTENT

ⓢ Supporting Information

The Supporting Information is available free of charge at https://pubs.acs.org/doi/10.1021/acsearthspace-chem.1c00116.

Sampling the rotational motion of a nonlinear molecule (PDF)

■ AUTHOR INFORMATION

Corresponding Author

Herma M. Cuppen − *Radboud University Nijmegen, Institute for Molecules and Materials, 6525 AJ Nijmegen, The Netherlands; van 't Hoff Institute for Molecular Sciences, University of Amsterdam, 1098 XH Amsterdam, The Netherlands;* ⓘ orcid.org/0000-0003-4397-0739; Email: h.cuppen@science.ru.nl

Authors

Adrien Fredon − *Radboud University Nijmegen, Institute for Molecules and Materials, 6525 AJ Nijmegen, The Netherlands*

Gerrit C. Groenenboom − *Radboud University Nijmegen, Institute for Molecules and Materials, 6525 AJ Nijmegen, The Netherlands;* ⓘ orcid.org/0000-0002-0920-3707

Complete contact information is available at:
https://pubs.acs.org/10.1021/acsearthspacechem.1c00116

Notes

The authors declare no competing financial interest.

■ REFERENCES

(1) Bacmann, A.; Taquet, V.; Faure, A.; Kahane, C.; Ceccarelli, C. Detection of complex organic molecules in a prestellar core: a new challenge for astrochemical models. *Astron. Astrophys.* **2012**, *541*, No. L12.

(2) Bacmann, A.; Faure, A. The origin of gas-phase HCO and CH₃O radicals in prestellar cores. *Astron. Astrophys.* **2016**, *587*, No. A130.

(3) Cernicharo, J.; Marcelino, N.; Roueff, E.; Gerin, M.; Jiménez-Escobar, A.; Muñoz Caro, G. M. Discovery of the methoxy radical, CH₃O, toward B1: dust grain and gas-phase chemistry in cold dark clouds. *Astrophys. J.* **2012**, *759*, No. L43.

(4) Jiménez-Serra, I.; Vasyunin, A. I.; Caselli, P.; Marcelino, N.; Billot, N.; Viti, S.; Testi, L.; Vastel, C.; Lefloch, B.; Bachiller, R. The Spatial Distribution Of Complex Organic Molecules In The L1544 Pre-Stellar Core. *Astrophys. J.* **2016**, *830*, No. L6.

(5) Fredon, A.; Cuppen, H. M. Molecular dynamics simulations of energy dissipation and non-thermal diffusion on amorphous solid water. *Phys. Chem. Chem. Phys.* **2018**, *20*, 5569.

(6) Fredon, A.; Radchenko, A. K.; Cuppen, H. M. Quantification of the Role of Chemical Desorption in Molecular Clouds. *Acc. Chem. Res.* **2021**, 745−753.

(7) Minissale, M.; Dulieu, F.; Cazaux, S.; Hocuk, S. Dust as interstellar catalyst I. Quantifying the chemical desorption process. *Astron. Astrophys.* **2016**, *585*, No. A24.

(8) Garrod, R. T.; Wakelam, V.; Herbst, E. Non-thermal desorption from interstellar dust grains via exothermic surface reactions. *Astron. Astrophys.* **2007**, *467*, 1103−1115.

(9) Fredon, A.; Lamberts, T.; Cuppen, H. M. Energy Dissipation and Nonthermal Diffusion on Interstellar Ice Grains. *Astrophys. J.* **2017**, *849*, 125.

(10) Habershon, S.; Markland, T. E.; Manolopoulos, D. E. Competing quantum effects in the dynamics of a flexible water model. *J. Chem. Phys.* **2009**, *131*, No. 024501.

(11) Abascal, J. L. F.; Vega, C. A general purpose model for the condensed phases of water: TIP4P/2005. *J. Chem. Phys.* **2005**, *123*, No. 234505.

(12) Zhu, S.; Robinson, G. Molecular dynamics study of liquid carbon monoxide. *Comput. Phys. Commun.* **1989**, *52*, 317.

(13) Lee, T. J.; Martin, J. M. L.; Taylor, P. R. An accurate ab initio quartic force field and vibrational frequencies for CH4 and isotopomers. *J. Chem. Phys.* **1995**, *102*, 254.

(14) Karssemeijer, L. J.; de Wijs, G. A.; Cuppen, H. M. Interactions of adsorbed CO_2 on water ice at low temperatures. *Phys. Chem. Chem. Phys.* **2014**, *16*, 15630−15639.

(15) Qu, C.; Conte, R.; Houston, P. L.; Bowman, J. M. "Plug and play" full-dimensional ab initio potential energy and dipole moment surfaces and anharmonic vibrational analysis for CH_4−H_2O. *Phys. Chem. Chem. Phys.* **2015**, *17*, 8172.

(16) Plimpton, S. Fast Parallel Algorithms for Short-Range Molecular Dynamics. *J. Comput. Phys.* **1995**, *117*, 1.

(17) Pantaleone, S.; Enrique-Romero, J.; Ceccarelli, C.; Ugliengo, P.; Balucani, N.; Rimola, A. Chemical Desorption versus Energy Dissipation: Insights from Ab Initio Molecular Dynamics of HCO· Formation. *Astrophys. J.* **2020**, *897*, No. 56.

(18) van Hemert, M. C.; Takahashi, J.; van Dishoeck, E. F. Molecular Dynamics Study of the Photodesorption of CO Ice. *J. Phys. Chem. A* **2015**, *119*, 6354.